Multiple Lenses of N-Isotopes Reveal Active Dissolved Organic Nitrogen Cycling in a Subtropical Estuary and Marginal Sea

Xiaosong Zhong[1,2], Maojun Yan[3], Wenqi Xu[1], Zhenwei Yan[1,2], Feng Xu[1,2], Shuhang Dong[1,2], Yu Xin[1,2]* and Xiaoyong Shi[2,4]*

[1] Frontiers Science Center for Deep Ocean Multispheres and Earth System and Key Laboratory of Marine Chemistry Theory and Technology, Ministry of Education, Ocean University of China, Qingdao, China, [2] College of Chemistry and Chemical Engineering, Ocean University of China, Qingdao, China, [3] School of Oceanography, Shanghai Jiao Tong University, Shanghai, China, [4] National Marine Hazard Mitigation Service, Beijing, China

Dissolved organic nitrogen (DON) is an important component of the marine nitrogen (N) inventory and plays an essential role in N cycling in global estuaries and marginal seas. Understanding DON cycling is important but challenging. Global estuaries and marginal seas are experiencing significant anthropogenic impacts and have intensive physical/biochemical gradients. Therefore, high-quality DON concentration and N-isotope (δ^{15}N–DON) data are very difficult to obtain. To enrich this knowledge, we take the Changjiang Estuary and the adjacent East China Sea shelf seas as a representative example and analyzed multiple isotopes and the concentrations of nitrate (NO_3^-), particulate nitrogen (PN), and DON. N isotopes combined with optimum multiparameter analysis proved to be very informative. This integrated analysis discriminates active DON production and consumption from a seemingly conservative distribution pattern of DON. The study area was divided into DON production zones 1 and 2 (P-zone 1 and 2) and DON consumption zones 1 and 2 (C-zone 1 and 2). For P-zone 1, the PN-originated DON elevated the δ^{15}N–DON, while in P-zone 2, the DON excreted by phytoplankton was characterized by low δ^{15}N and lowered δ^{15}N–DON. DON consumption occurred in the NO_3^- depleted surface waters (C-zone 1) as well as the shelf middle and bottom waters (C-zone 2). This study discovers and consolidates the active and dynamical zoning of DON cycling from the estuary to the offshore marginal sea and establishes a useful means that is of valuable reference to DON cycling studies in global estuaries and marginal seas.

Keywords: dissolved organic nitrogen, N-isotopes, marginal sea, Changjiang Estuary, OMP analysis, nutrient biogeochemistry

1 INTRODUCTION

Dissolved organic nitrogen (DON) is often the dominant form of fixed N in global oceans (Berman and Bronk, 2003; Jani and Toor, 2018; Lim et al., 2019). DON has been recognized as a potential N source for primary production, *i.e.*, bacteria and phytoplankton, in the marine environment (Bronk et al., 2007; Sipler and Bronk, 2015). Thus, DON dynamics is one of the key building blocks for a

comprehensive understanding of the nutrient biogeochemical cycle. The role of DON in N cycling has been investigated in terms of its production and consumption. Accumulated datasets of DON concentration and its isotope (δ^{15}N–DON) have suggested that DON significantly affects nutrient biogeochemical cycling in most tropical and subtropical surface waters (Letscher et al., 2013; Knapp et al., 2018; Zhang et al., 2020). However, for estuaries and marginal seas, there are a few limited studies on DON bioavailability and its contribution to local N cycling. There are only rare reports on DON cycling based on δ^{15}N–DON, especially where the dissolved inorganic nitrogen (DIN) overwhelms DON in concentration. It becomes particularly challenging to study DON cycling when intensive physical gradients, vigorous biological activities, and significant anthropogenic activities co-exist and join to impact DON cycling in estuaries and marginal seas. What is the major cycling process of DON and how does DON cycling affect the N cycling and nutrient biogeochemistry in estuaries and marginal seas? A substantial amount of terrestrial-derived DON input into estuaries and marginal seas is transported into the open ocean by offshore currents. What is the fate of terrestrial-derived DON from estuaries to marginal seas? The answers to the above-mentioned questions would provide valuable clues to understanding the land–ocean interactions under the current global climate conditions. Therefore, we specifically highlight DON biogeochemical cycling in estuaries and marginal seas and present a case study of the Changjiang Estuary and the adjacent East China Sea shelf areas (CEECS).

The Changjiang Estuary is a well-known, large, river-dominated estuary that is affected by one of the most developed areas in China. The conveyed nutrients, marked by various N species, have significantly increased with the industrialization and urbanization in the river basin (Dai et al., 2011; Liu et al., 2018; Zhang et al., 2021). These anthropogenic loadings are driving the CEECS N budget beyond its natural resilience boundaries (Moon et al., 2021). The excess N could stimulate the growth of phytoplankton and increase the production of phytoplanktonic organic matter, which could further exacerbate local water hypoxia through organic matter degradation and the associated oxygen consumption (Wang et al., 2016). Thus, N cycling in the CEECS has attracted increasing attention in recent years. Published studies have focused mainly on the N cycling reflected by nitrate (NO$_3^-$), particulate nitrogen (PN), and their isotopes (Liu et al., 2009; Umezawa et al., 2014; Gao et al., 2020). Neither the quantity nor the quality of DON concentration and δ^{15}N–DON is adequate to elucidate the DON sources, sinks, and cycling in the CEECS (Zhang et al., 2003; Zhang et al., 2015; Liu et al., 2016; Kwon et al., 2018). Recent findings suggest that DON appears to be conservative in the CEECS, given its small variances in concentration. Such a DON distribution pattern seems to suggest that physical mixing processes are the major driver rather than biochemical processes (Kwon et al., 2018; Kim et al., 2020). Besides this, the high DIN concentration and comparatively low DON concentration in the CEECS create

difficulties in acquiring the DON concentration and δ^{15}N–DON (Knapp et al., 2005). As a result, DON cycling in the CEECS has not been clearly recognized or explained yet.

It is difficult to reveal DON cycling in the complicated surroundings of CEECS only through the DON concentration dataset. The multiple-isotope approach developed in recent years provides a useful means of studying marine N cycling processes in the CEECS—for example, in a previous study, we have identified the NO$_3^-$ sources and traced its transformation processes as well for evaluating the relative importance of each process in the CEECS by the compositions of dual isotopes of NO$_3^-$ (Zhong et al., 2020). The changes in isotopic signals can reflect the transformation processes between different forms of N, *i.e.*, assimilation, nitrification, and remineralization (Liu et al., 2020). In this study, we presented the DON concentration and multiple N-isotope datasets (detailed description in **Supplementary Information Text S1**) and described the spatial variation patterns of different forms of N in the CEECS under the joint impacts of physical and biochemical processes. Then, the isotopic fractionation factors of DON production and consumption were estimated. We aim to disentangle the field coupling of DIN, DON, and PN and further clarify the impacts of DIN and PN on the biogeochemical cycling of DON. Finally, a conceptual diagram of DON cycling in the estuary and marginal sea was constructed. This study will serve as a valuable reference for studying DON cycling in global estuaries and shelf marginal seas that are characterized by rigorous physical gradients and biological processes.

2 MATERIALS AND METHODS

2.1 Sampling
Samples were collected from the CEECS during a cruise abroad the R/V *Science III* from July 10 to 20, 2018 (**Figure 1**). The temperature, salinity, and depth were measured by CTD (Seabird 911 Plus, USA). Seawater samples were collected in 12-L Niskin bottles attached to the CTD rosette, and the sampling depths were set as the surface (3 to 4 m deep), middle (about 50% depth), and bottom (3–5 m above the seabed) layers. Upon retrieval, the dissolved oxygen was analyzed using the Winkler titration method (with a precision of 5×10^{-3} mg/L). Samples for nutrients, total dissolved nitrogen (TDN), and stable N (and O for NO$_3^-$) isotope analysis were filtered immediately through 0.2-µm polycarbonate filters (Φ = 47 mm, Millipore, USA) on a Nalgene filter and then were stored in acid-cleaned and sample-rinsed high-density polyethylene bottles (125 ml, Thermo Co., USA). The filters for suspended particulate matter (SPM), particulate organic carbon (POC), particulate nitrogen (PN), and the corresponding δ^{13}C (relative to V-PDB) and δ^{15}N (relative to air N$_2$) measurements were filtered through pre-combusted (500°C for 5 h) and pre-weighed 0.7-µm GF/F filters (Φ = 25 mm, Whatman, UK). After filtration, the filters were dried on board at 45°C for 24 h. All the samples were stored at −20°C until further analysis was carried out in the laboratory.
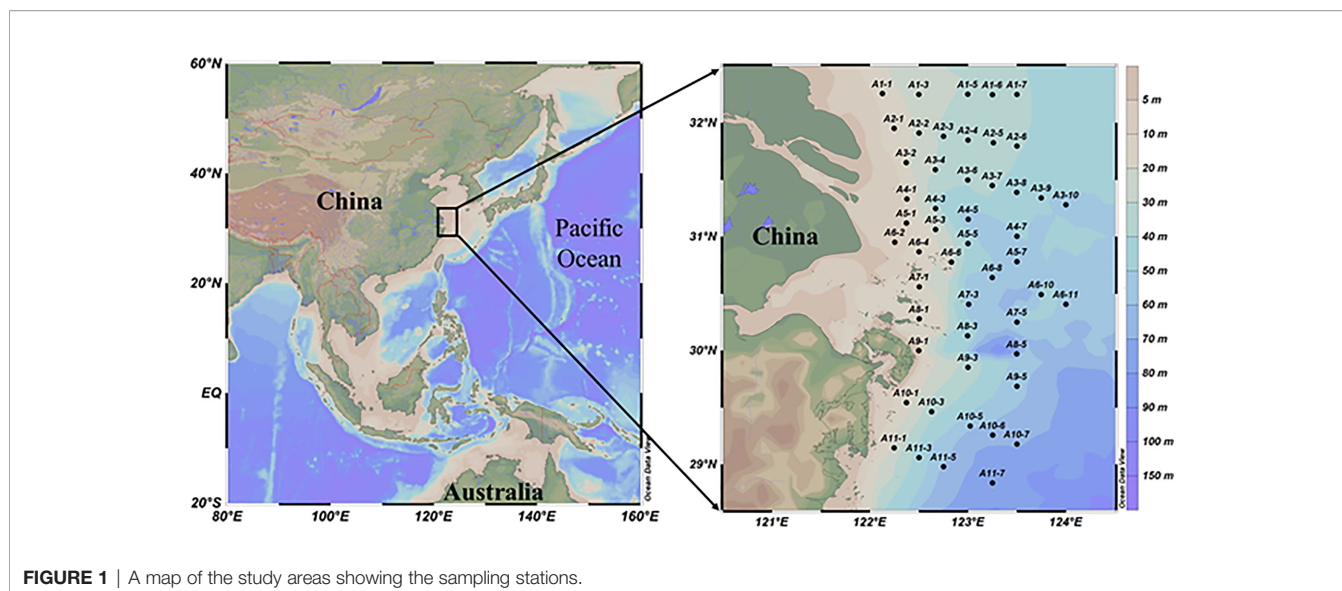
FIGURE 1 | A map of the study areas showing the sampling stations.

2.2 Chemical Analysis
2.2.1 Dissolved Nutrient Analysis
The concentrations of seawater phosphate, dissolved silicate, nitrate (NO_3^-), and nitrite (NO_2^-) were measured using the spectrophotometry method (Hansen and Koroleff, 2007) on a flow injection analyzer (QuAAtro, Seal Analytical, Germany). The detection limits were 0.04, 0.09, 0.02, and 0.005 μmol/L, respectively. Ammonium (NH_4^+) was measured immediately upon the retrieval of water samples following a procedure described by Holmes et al. (1999). However, NH_4^+ in about 30% of samples was below the detection limit of the method (<0.006 μmol/L). Given our inability to determine the $\delta^{15}N$ of the low-concentration NH_4^+ in our samples (averaging 0.20 ± 0.33 μmol/L), we did not subtract the concentration or the $\delta^{15}N$ of NH_4^+ from DON and $\delta^{15}N$ of DON. Thus, the DON concentration here was defined as the difference between TDN and $NO_3^- + NO_2^-$. The concentration of $NO_3^- + NO_2^-$ was quantified using the chemiluminescence method (Braman and Hendrix, 1989) using a NO_x^- analyzer (200 EU, Teledyne, USA); the analytical precision is better than ± 0.1 μmol/L. The TDN was first converted into NO_3^- using the persulfate oxidation method (Hansen and Koroleff, 2007). Briefly, 1 ml of persulfate oxidizing reagent (POR, 1.5 g NaOH + 3 g H_3BO_3 + 5 g $K_2S_2O_8$ in 100 ml low-DON Milli-Q water) was added to 10 ml of seawater sample in a precleaned and precombusted (500°C for 5 h) 15-ml quartz tube with a Teflon-lined cap. The screw caps were closed tightly, followed by autoclaving for 30 min. After digestion, the sample was quantified using the chemiluminescence method. The DON concentration was calculated by subtracting the concentrations of $NO_3^- + NO_2^-$ and the N-blank of POR.

2.2.2 Stable Isotope Analysis
The $\delta^{15}N - NO_3^-$, $\delta^{18}O - NO_3^-$ and $\delta^{15}N$-TDN were determined using the denitrifier method (Sigman et al., 2001; Weigand et al., 2016) on an isotope ratio mass spectrometer (PreCon-IRMS, IsoPrime, UK) coupled with a nitrous oxide

extraction system. Three reference materials, IAEA-NO-3 ($\delta^{15}N -NO_3^- = 4.7\%$ and $\delta^{18}O - NO_3^- = 25.8\%$), USGS-34 ($\delta^{15}N - NO_3^- = 1.8\%$ and $\delta^{18}O - NO_3^- = 27.9\%$), and USGS-35 ($\delta^{15}N - NO_3^- = 2.7\%$ and $\delta^{18}O - NO_3^- = 57.7\%$), were used for calibration. For data quality assurance, an internal standard of hadal water from the Mariana Trench (8,000 m in depth, $\delta^{15}N - NO_3^- = 5.0 \pm 0.2\%$, and $\delta^{18}O - NO_3^- = 2.0 \pm 0.2\%$ was analyzed with each batch of samples. Replicate measurements were performed. The analytical precision was ± 0.2‰ or better for $\delta^{15}N$ and ± 0.5‰ or better for $\delta^{18}O$. Since both NO_3^- and NO_2^- were reduced to N_2O by the "denitrifier method," we analyzed the samples for $\delta^{15}N - NO_3^-$ and $\delta^{18}O - NO_3^-$ by using sulfamic acid to remove NO_2^- prior to NO_3^- conversion to N_2O (Granger and Sigman, 2009). To evaluate the oxidation efficiency and quantify the isotope deviation caused by the POR-associated N blank, the reference material IAEA-600 ($\delta^{15}N = 1.0‰$) and the POR were autoclaved and measured with each batch of $\delta^{15}N$-TDN samples. The $\delta^{15}N$–DON was calculated from the isotopic mass balance equation (Eqs. 1 and 2).

$$\delta^{15}N_{DON} = \frac{\delta^{15}N_{TDN} \times [TDN] - \delta^{15}N_{NO_3^-+NO_2^-} \times [NO_3^- + NO_2^-]}{[DON]}$$

(1)

where the TDN concentration was calculated by subtracting the N-blank concentration of POR.

$$\delta^{15}N_{TDN} \times [TDN]$$
$$= \frac{\delta^{15}N_{TDN'} \times [TDN'] \times 11 - \delta^{15}N_{POR} \times [POR] \times 1}{10}$$

(2)

2.2.3 SPM Analysis
The SPM was determined as the weight difference between the dried filters and their counterparts before filtration. The C and N

content and the corresponding δ^{13}C (relative to V-PDB) and δ^{15}N (relative to air N$_2$) were measured at the University of California Davis Stable Isotope Facility. The mean standard deviation for reference material replicates was ± 0.06‰ for δ^{13}C and ± 0.08‰ for δ^{15}N.

2.3 Data Analyses

2.3.1 Optimum Multiparameter Analysis

Optimum multiparameter (OMP) analysis, described by Tomczak and Large (1989), is a water mass inverse model based on linear mixing that is used to find the relative abundances of different source water types (SWT). It finds a solution that best reproduces the observed data and minimizes the residuals in a non-negative least square sense. The OMP was constructed based on two main physically realistic constraints: (i) the study area can be fully represented by the combination of predefined SWT and (ii) the contribution of SWT must be non-negative and add up to 100%. The OMP can be summarized in a matrix form as follows:

$$GX = d + R \qquad (3)$$

where G is the matrix with the property values of SWT, X is the vector of proportional contribution of each SWT to be solved, d is the vector of the observed data, and R is the residual vector.

For the analysis, two conservative (temperature and salinity) and four semi-conservative (oxygen, phosphate, nitrate, and silicate) properties were used to define SWT (Poole and Tomczak, 1999; Budillon et al., 2003; de Carvalho Ferreira and Kerr, 2017). However, as the water masses evolve, the concentrations of these parameters are modified by biogeochemical processes, such as assimilation, remineralization, and respiration processes in the CEECS. The impact of biogeochemical processes can no longer be disregarded and have to be included in the analysis. The extended OMP analysis was applied to minimize these effects by adding the Redfield ratio item supplied by OMP files (a detailed description is available in **Supplementary Information Text S2**). The SWT parameter values (a detailed description is available in **Supplementary Information Text S3** and **Supplementary Information Text S4**) used are summarized in **Table 1**.

Sensitivity tests were performed to test the impact of uncertainties on the results. First, we simply changed the weights. The weights were from literature (de Carvalho Ferreira and Kerr, 2017; Zhou et al., 2018), experience, OMP

files, and calculation (a detailed description is available in **Supplementary Information Text S2**). The best results were obtained by using the calculated weights (**Table 1**), which not only effectively represent the varieties in the formation region but also hold the minor mass balance residuals. All mass balance residuals were lower than 8%, only four residuals were higher than 5%, and 74% of the residuals were lower than 1% (**Supplementary Figure S2**). According to the mass balance residuals, the results of the OMP analysis were reliable (Tomczak and Large, 1989). Furthermore, we analyzed the same dataset by adding and subtracting the standard deviation based on the observed variability (**Table 1**) from the properties of the SWT (matrix G) to assess the robustness of the solution. Most of the standard deviations of the solutions were <10%. Thus, the uncertainties in the OMP runs were considered acceptable (Gasparin et al., 2014; Zhou et al., 2018).

2.3.2 Expected DON Concentration Dominated by Physical Mixing Processes

Based on the relative abundances of different SWT, the expected DON concentration and δ^{15}N–DON affected only by the physical mixing can be calculated as follows:

$$[DON]_{ex}= [DON]_{CDW} \times X_{CDW} + [DON]_{YSMW} \times X_{YSMW} + [DON]_{TWC} \times X_{TWC} + [DON]_{KSW} \times X_{KSW} + [DON]_{KBBCNT} \times X_{KBBCNT} \qquad (4)$$

$$\delta^{15}N_{ex} \times [DON]_{ex}= \delta^{15}N_{CDW} \times [DON]_{CDW} \times X_{CDW} + \delta^{15}N_{YSMW} \times [DON]_{YSMW} \times X_{YSMW} + \delta^{15}N_{TWC} \times [DON]_{TWC} \times X_{TWC} + \delta^{15}N_{KSW} \times [DON]_{KSW} \times X_{KSW} + \delta^{15}N_{KBBCNT} \times [DON]_{KBBCNT} \times X_{KBBCNT} \qquad (5)$$

We further calculated the deviation of observed values from calculated values. The deviation is defined in terms of *Error-DON*.

2.3.3 Steady-State Model

The steady-state model is frequently used to interpret the N isotope data from the ocean (Sigman et al., 2009).

For the reactant N pool:

$$\delta^{15}N_{reactant} = \delta^{15}N_{initial} +^{15}\epsilon \times (1 - f) \qquad (6)$$

TABLE 1 | Source water type (SWT) definitions for the Taiwan Warm Current (TWC), Kuroshio Surface Water (KSW), Changjiang Diluted Water (CDW), Yellow Sea Mixed Water (YSMW), Kuroshio Bottom Branch Current North of Taiwan (KBBCNT), and parameter weights used in the optimum multiparameter analysis for this study.

SWT[a]	Salinity	Temperature (°C)	Dissolved oxygen (μmol/L)	Phosphate (μmol/L)	Nitrate (μmol/L)	Dissolved silicate (μmol/L)
TWC	33.20 ± 0.12	24.5 ± 1.8	149.6 ± 2.3	0.6 ± 0.01	6.7 ± 0.8	14.2 ± 1.0
KSW	32.60 ± 0.56	27.4 ± 1.5	216.8 ± 3.7	0.1 ± 0.04	0.4 ± 0.2	2.6 ± 0.1
CDW	21.00 ± 0.12	25.0 ± 1.1	185.9 ± 1.0	1.3 ± 0.01	60.4 ± 0.02	56.4 ± 0.3
YSMW	32.20 ± 0.49	23.3 ± 1.2	149.0 ± 3.1	0.2 ± 0.06	8.6 ± 1.2	11.1 ± 1.5
KBBCNT	35.15 ± 0.06	18.0 ± 1.4	168.7 ± 0.2	0.9 ± 0.08	8.8 ± 1.3	13.6 ± 1.7
Weight	15.86	15.86	0.56	1.04	1.54	1.26

[a]Considering that the determined relative contribution of core water masses is to explore the regulation of physical process on the spatial distribution of dissolved organic nitrogen, using the extremum of each water mass is unreasonable. The parameters of SWT were obtained from the end-member of water masses in the study area.

For the product N pool:

$$\delta^{15}N_{product} = \delta^{15}N_{initial} - {}^{15}\epsilon \times f \qquad (7)$$

where f is the fraction of the reactant remaining.

3 RESULTS

3.1 Hydrographic Characteristics

The distributions of temperature and salinity are shown in **Figure 2**. The seawater temperature, ranging from 18.3 to 28.8°C with an average of 23.3 ± 2.9°C for the entire water column, showed significant variations from surface to bottom. The salinity varied from 20.7 to 34.6, with an average of 32.1 ± 2.9, showing an increasing trend from surface to bottom. In general, the distributions of seawater temperature and salinity demonstrated that the areas of coastal low-salinity water (<31) became much larger at the surface than in the bottom layer and that cold and salty seawater (>34) moved northward on the East China Sea shelf areas at the bottom. A cold and salty belt (>34) along the south study area was observed in the middle layer, indicating an upwelling of the northward-moving subsurface waters (**Figures 2B, E**). Based on this investigation and previous studies (Mao, 1964; Su and Weng, 1994; Chen, 2009; Yang et al., 2011), five major water masses were identified in the CEECS (**Supplementary Figure S1**): (i) the high-temperature (23–29°C) and high-salinity (33.2–34.2) Taiwan Warm Current (TWC), (ii) the low-temperature (18–21°C) and salty (>34.3) Kuroshio Bottom Branch Current North of Taiwan (KBBCNT), (iii) the high-temperature (23–29°C) and high-salinity (S >34.2) but nutrient-depleted Kuroshio Surface Water (KSW), (iv) the relatively low-temperature (<23°C) Yellow Sea Mixed Water (YSMW), and (v) the low-salinity (<31) Changjiang Diluted Water (CDW) in coastal areas. Shelf Mixed Water (SMW) was recognized in the study area during the cruise period. To specify the expansion form of CDW, the isohaline of 26 (Hou et al., 2021) was defined as the core area of CDW, and the isohaline of 31 was defined as the boundary of CDW.

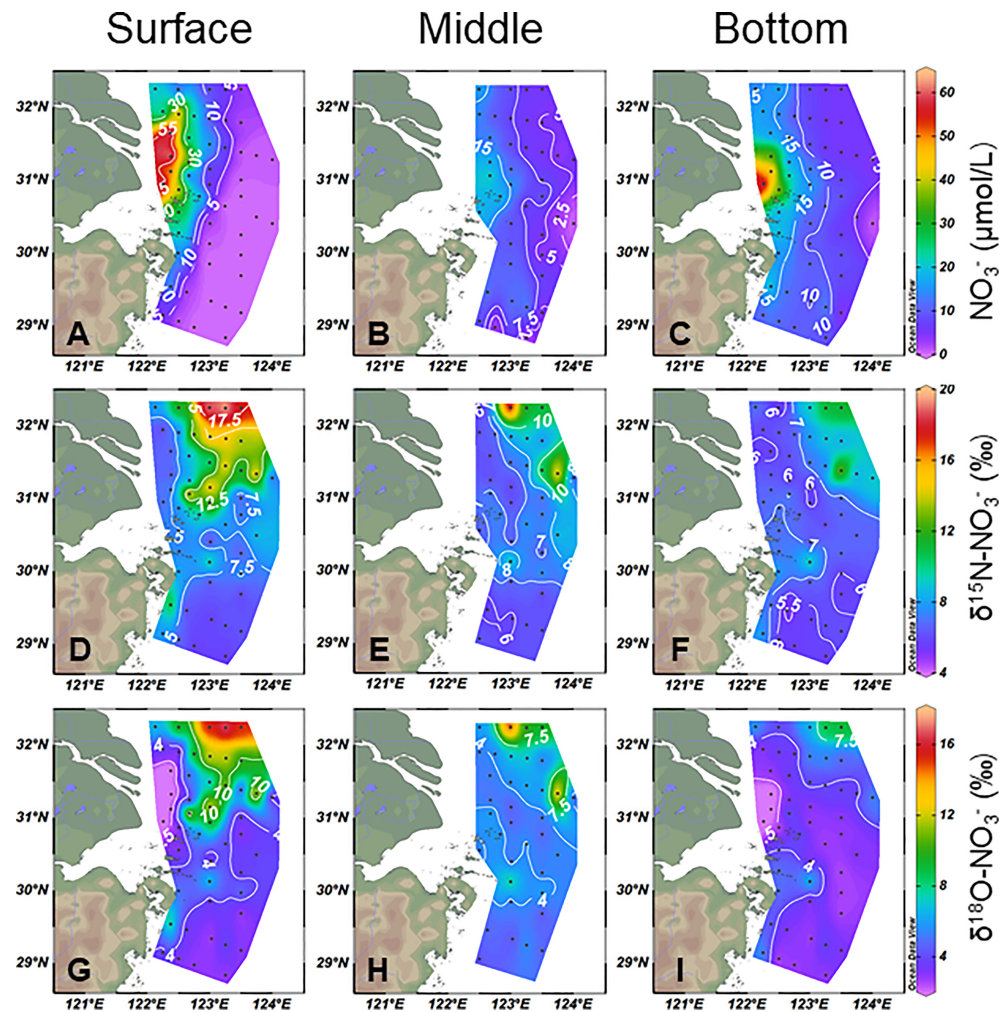### 3.2 NO_3^- Concentration, $\delta^{15}N – NO_3^-$, and $\delta^{18}O – NO_3^-$

In the core area of CDW, the NO_3^- was rich (16.4–63.8 µmol/L) and relatively uniform in vertical distribution (**Figures 3A–C**). Both $\delta^{15}N – NO_3^-$ (5.7 – 7.4 ‰) and $\delta^{18}O – NO_3^-$ (1.0 – 2.9 ‰) were relatively light (**Figures 3D–I**). In the flow direction of CDW, the NO_3^- concentration decreased rapidly and became heavier in $\delta^{15}N – NO_3^-$ (7.6 – 19.7 ‰) and $\delta^{18}O – NO_3^-$ (13.3 – 16.8 ‰). Along with the offshore increase of salinity >31, the NO_3^- concentration was comparatively lower in the surface layer than in the bottom layer and decreased to exhausted in surface water (**Figure 3A**). Thus, no credible $\delta^{15}N – NO_3^-$ and $\delta^{18}O – NO_3^-$, data were obtained. In the bottom layer, the KBBCNT had relatively homogeneous $\delta^{15}N – NO_3^-$ and $\delta^{18}O – NO_3^-$ values of 5.5 ± 0.44 and 2.5 ± 0.29‰, respectively (**Figures 3F, I**).

3.3 DON Concentration and $\delta^{15}N–DON$

In the study area, NO_3^- accounted for 52 ± 27% of TDN and DON accounted for 45 ± 26%. Therefore, DON was equally
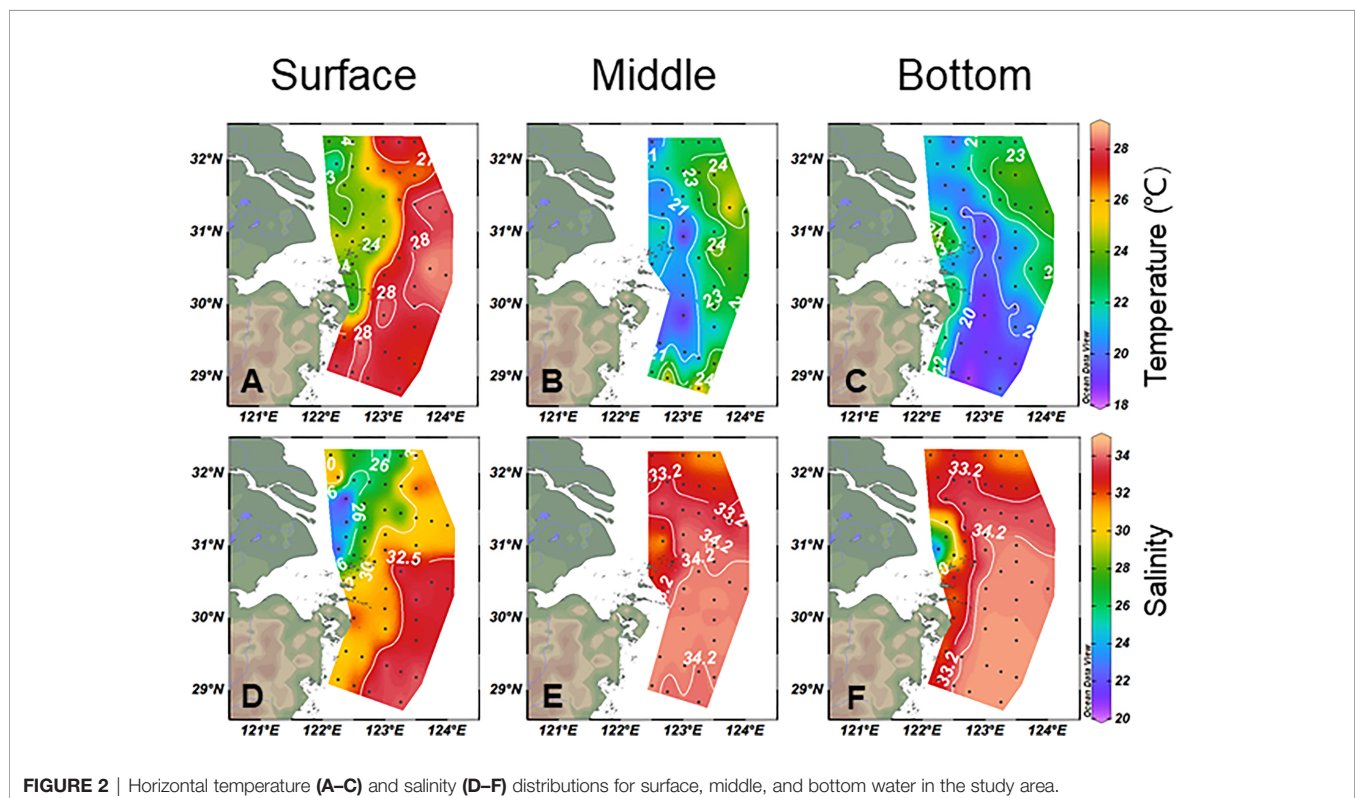
FIGURE 2 | Horizontal temperature **(A–C)** and salinity **(D–F)** distributions for surface, middle, and bottom water in the study area.

FIGURE 3 | Horizontal NO_3^- **(A–C)**, $\delta^{15}N – NO_3^-$ **(D–F)**, and $\delta^{18}N – NO_3^-$ **(G–I)** distributions at the surface, middle, and bottom water in the study area.

important as NO_3^- in local N cycling. The DON concentration ranged from 3.6 to 9.2 μmol/L in the study area. It was 6.8 ± 1.3 μmol/L at the surface, 5.3 ± 0.86 μmol/L at the middle, and 5.2 ± 0.91 μmol/L at the bottom (**Figures 4A–C**). The $\delta^{15}N–DON$ was varied from −1.4 to 7.4‰, with an average of 3.7 ± 1.6‰. Generally, the high DON concentration corresponded to a lower $\delta^{15}N–DON$ and *vice versa*.

3.4 PN Concentration and $\delta^{15}N–PN$

The concentration of PN averaged 7.2 ± 8.3 μmol/L. In the core area of CDW, the PN concentration exceeded 20 μmol/L but decreased to 5 μmol/L at ~50 m isobath. In the offshore stations, the PN concentration was low and decreased toward the southeast with a small gradient (**Figures 5A–C**). In general, the $\delta^{15}N–PN$ increased from coastal areas to offshore (**Figures 5D–F**). The $\delta^{15}N–PN$ in the surface layer had a comparatively broader range (−0.99 to 7.6‰, 4.0 ± 2.2‰) than in the middle (0.1 to 5.9‰, 3.9 ± 1.4‰) and bottom layers (0.39 to 6.1‰, 3.0 ± 1.3 ‰).

4 DISCUSSION

4.1 Influences of Water Masses Mixing on DON Spatial Distribution
4.1.1 Water Masses Mixing in the CEECS
The OMP analysis was used to determine the relative contribution of the core water masses in the CEECS (**Supplementary Figure S3**). CDW flowed in the east, southeast, and especially northeast directions in the surface layer, which is consistent with previous studies (Liu et al., 2021). In the surface water of the northern study area (transect A1–A4), there is a weak bidirectional northwestward extrusion of CDW over Subei Shoal. From there, the contribution of CDW gradually decreases with increasing distance from the coastal area. YSMW and KSW are present as high contributions in the northern nearshore area and offshore area, respectively. In the southern study area, KSW contributes more than 50% of the total water in the entire surface layer. The remaining contribution
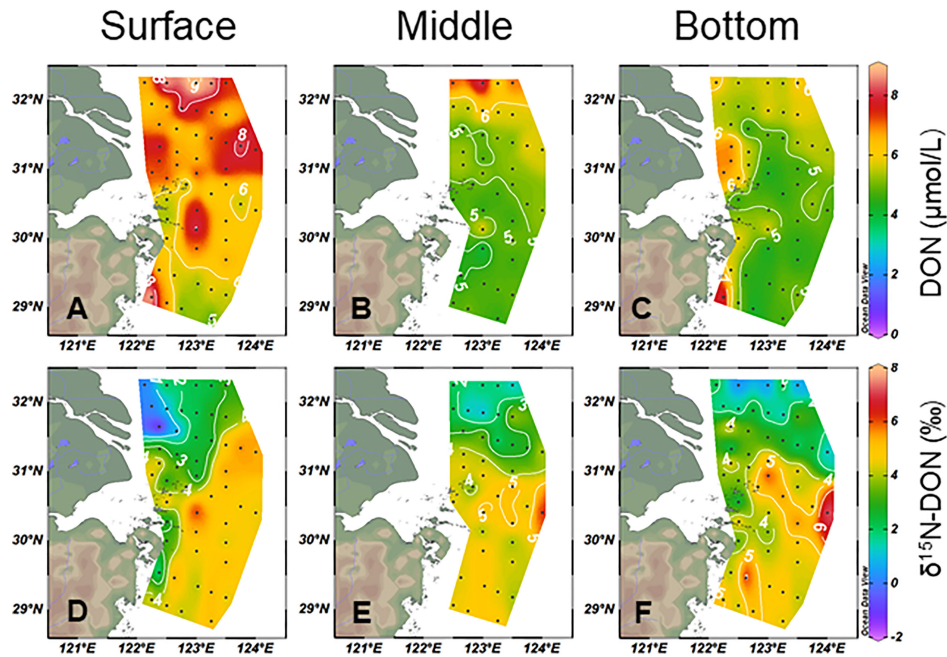
FIGURE 4 | Horizontal dissolved organic nitrogen (DON) **(A–C)** and δ^{15}N–DON **(D–F)** distributions from the surface, middle, and bottom water in the study area.

comes mainly from TWC and CDW in the nearshore area. The bottom water in the study region is a mixture of TWC, KBBCNT, and YSMW. KBBCNT contributes the most. YSMW is confined to the northern part of the study area.

4.1.2 Zoning of DON Turnover

The difference between measured values and calculated values (Eq. 4) based on OMP results was defined as *Error-DON*. When the measured values are equal to the calculated values, it means
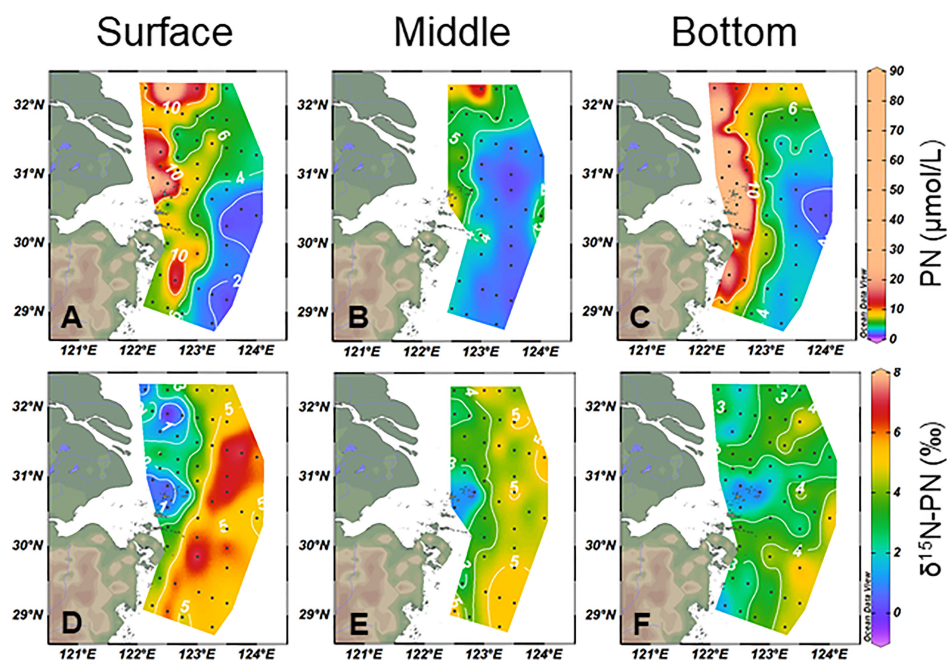

FIGURE 5 | Horizontal particulate nitrogen (PN) **(A–C)** and δ^{15}N–PN **(D–F)** distributions from the surface, middle, and bottom water in the study area.

that the physical mixing of the water masses is the dominant factor controlling the spatial distribution of DON. A positive *Error-DON* corresponds to the net production of DON, and a negative *Error-DON* corresponds to the net consumption. To identify the DON dynamics in different water masses, *Error-DON* versus measured DON was plotted (**Figure 6A**). We found that both net production and net consumption of DON occurred in every water mass. In the study area, the *Error-DON* averaged 10.7 ± 8.6% for DON net production and −9.0 ± 7.0% for net consumption. Interestingly, in all the sampling sites ($n = 138$), there were equal numbers of DON net production ($n = 69$) and consumption sites ($n = 69$). This result could explain why there is a misleading impression that DON exhibited a conservative behavior in general over the CEECS (from the river mouth to the offshore area up to 800 km; Kwon et al., 2018). In actuality, we captured the non-conservative behavior (active biochemical cycling) of DON *via* the OMP analysis.

The positive *Error-DON* values were distributed mainly in the southern coastal areas and northern part of the study area (see the diamonds in **Figure 6B**). In these DON net production sites, the relationship between $\delta^{15}N$–DON and DON concentration was categorized into two patterns. In the NO_3^- rich euphotic layer (9.1 ± 9.2 μmol/L, P-zone 1), the DON correlated negatively with

$\delta^{15}N$–DON ($R^2 = 0.57$, $p \leq 0.001$, $n = 29$, **Figure 7A**), while in the coastal middle and bottom waters where the SPM was high (64.0 ± 90.1 mg/L, P-zone 2), the DON correlated positively with $\delta^{15}N$–DON ($R^2 = 0.29$, $p \leq 0.001$, $n = 37$, **Figure 7B**). The two patterns indicated that there were two different mechanisms of DON production in the two zones. In P-zone 1, the $\delta^{15}N$ of the produced DON decreased the $\delta^{15}N$–DON in the water column. Conversely, the $\delta^{15}N$ of the produced DON elevated the $\delta^{15}N$–DON in the water column in P-zone 2. A detailed explanation is provided in **Section 4.2**.

The negative *Error-DON* values were concentrated mainly in the southern part of the study area and part of the northern bottom layer (see dots in **Figure 6B**). Based on the distribution of net consumption sites and the apparent oxygen utilization (AOU), we classified the net consumption sites into two zones: (i) C-zone 1, where the AOU values were negative (AOU = −0.12 ± 0.68 mg/L, $n = 17$), and (i) C-zone 2, where the AOU values were positive (AOU = 3.17 ± 0.69 mg/L, $n = 36$). A negative correlation was observed between the AOU and DON concentration ($R^2 = 0.28$, $p = 0.001$, $n = 36$, **Supplementary Figure S5A**). With the assistance of multiple N-isotopic signatures, we determined the most plausible turnover processes for DON in each zone.
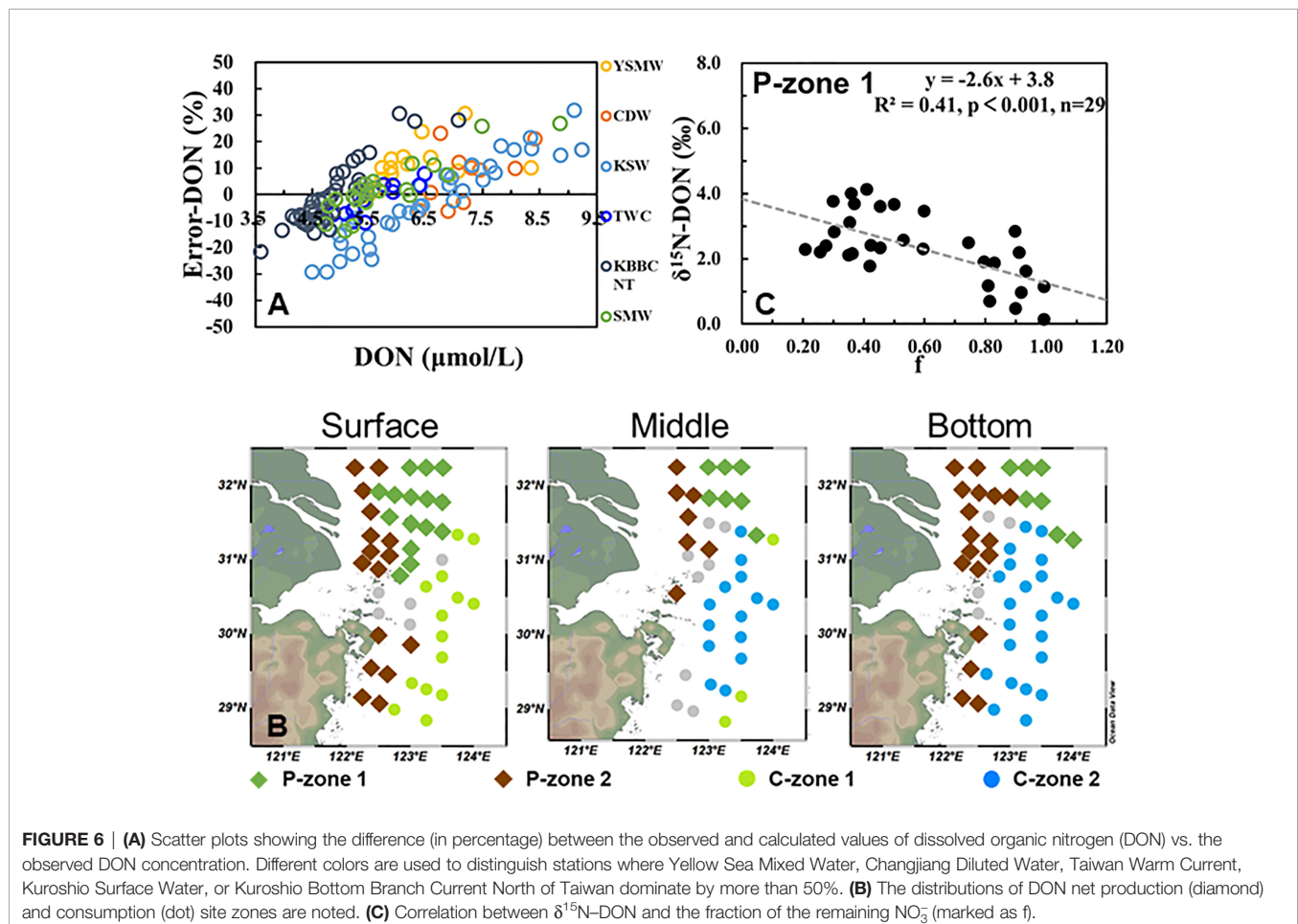
FIGURE 6 | **(A)** Scatter plots showing the difference (in percentage) between the observed and calculated values of dissolved organic nitrogen (DON) vs. the observed DON concentration. Different colors are used to distinguish stations where Yellow Sea Mixed Water, Changjiang Diluted Water, Taiwan Warm Current, Kuroshio Surface Water, or Kuroshio Bottom Branch Current North of Taiwan dominate by more than 50%. **(B)** The distributions of DON net production (diamond) and consumption (dot) site zones are noted. **(C)** Correlation between $\delta^{15}N$–DON and the fraction of the remaining NO_3^- (marked as f).
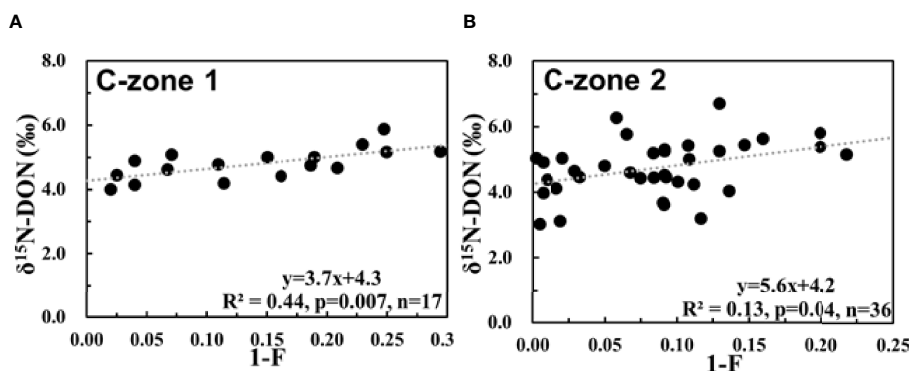
FIGURE 7 | **(A)** Relationship between δ^{15}N-dissolved organic nitrogen (DON) and 1-F in C zone 1. **(B)** Relationship between δ^{15}N-DON and 1-F in C zone 2. The variable "F" is the fraction of the DON remaining.

4.2 Net DON Production in CEECS

4.2.1 DON Production in NO_3^- Rich P-Zone 1

DON can be released through the autochthonous biological process of extracellular exudate production by phytoplankton (Bronk, 2002). The surface photosynthetic sources for DON in the Eastern Tropical South Pacific euphotic zone (Knapp et al., 2018) and the South China Sea surface waters (Zhang et al., 2020) were suggested through a positive correlation between the DON stock and chlorophyll-*a* at these sites. Unfortunately, we lack chlorophyll-*a* data. However, the NO_3^- dual-isotope variation pattern in P-zone 1 is capable of characterizing the phytoplankton activity. In P-zone 1, the observed NO_3^- concentrations (9.1 ± 9.2 μmol/L) were lower than the expected values (15.7 ± 10.7 μmol/L), while both $\delta^{15}N - NO_3^-$(12.1 ± 3.8 ‰) and $\delta^{18}O - NO_3^-$(8.9 ± 4.1 ‰) were heavier than the expected isotope ratios $\delta^{15}N - NO_3^-$: 6.0 ± 0.04 ‰ and $\delta^{18}O - NO_3^-$: 2.8 ± 0.7 ‰ In other words, NO_3^- was partially consumed accompanied by the enrichment of $\delta^{15}N - NO_3^-$ and $\delta^{18}O - NO_3^-$ in P-zone 1. This suggests the dominance of NO_3^- assimilation by phytoplankton (Zhong et al., 2020). The co-variation of NO_3^- dual isotopes fits a 1:1 line ($R^2 = 0.96$, $p \leq 0.001$, $n = 29$, **Supplementary Figure S6A**), as also expected for NO_3^- assimilation by phytoplankton (Granger et al., 2004). A positive correlation between NO_3^- consumption and DON concentration ($R^2 = 0.58$, $p \leq 0.001$, $n = 29$, **Supplementary Figure S6B**) suggested the net DON production at these sites as well. In NO_3^- rich surface waters like P-zone 1, phytoplankton preferentially consume ^{14}N relative to ^{15}N (Sigman and Fripiat, 2019). The isotope effect for NO_3^- assimilation produces photosynthetic biomass (which, in turn, produces DON) with a relatively low δ^{15}N (Knapp et al., 2018). Thus, the phytoplankton-sourced DON may hold a relatively low δ^{15}N value in P-zone 1.

The isotope effect is a key parameter that associates NO_3^- assimilation to the ^{15}N/^{14}N of NO_3^- and DON. Given the fact that NO_3^- (the reactant) can be continuously replenished by nitrification (Zhong et al., 2020), a steady-state model (Eq. 7, applied to the product N pool) is more appropriate to estimate the isotope effect ($^{15}\epsilon_{phy}$) during DON production in P-zone 1.

The slope of the linear regression between the δ^{15}N–DON and the fraction of NO_3^- remaining in the water column after NO_3^- assimilation yielded an estimate for $^{15}\epsilon_{phy}$ of 2.6 ± 0.6‰ (**Figure 6C**). The $\delta^{15}N_{initial}$ (y-intercept) was 3.8 ± 0.4‰, which was consistent with the average value (3.8 ± 1.0‰) of the expected δ^{15}N values (theoretical value under physical mixing; Eq. 5) for DON in P-zone 1. This result validated the application of the steady-state model, and the addition of phytoplankton-sourced δ^{15}N–DON decreased the δ^{15}N–DON in the water column.

4.2.2 DON Production in High-SPM P-Zone 2

Approximately 87% of the annual particulate load from Changjiang River is discharged in summer (Zhu et al., 2011). The P-zone 2 is a high-SPM (64.0 ± 90.1 mg/L) region. High SPM reduces light penetration in the water column and suppresses the photosynthesis process and primary production (He et al., 2017). From the perspective of $\delta^{15}N - NO_3^-$, the δ^{15}N $-NO_3^-$ (average of 6.6 ± 0.9‰) exhibited a homogeneous behavior in P-zone 2, suggesting that it was unlikely to be an occurrence of intensive phytoplankton assimilation. Thus, the phytoplankton-sourced autochthonous DON was not the dominating source of DON in P-zone 2, even though nutrients were rich in this area. PN and DON are the two main organic N species in the water column. In CEECS, PN was significantly controlled by SPM transport ($R^2 = 0.98$, $p \leq 0.001$, $n = 40$, **Supplementary Figure S7**). SPM (PN) transport and estuarine physical mixing are two independent processes (Gao et al., 2020). More than half of the fine-grained particles are temporarily deposited near the estuary in P-zone 2 (Chen et al., 2017). Thus, there are possibilities that PN and DON pools interacted during transportation in P-zone 2. An inter-transformation between the two most important organic N pools may have occurred (Gebhardt et al., 2005) and altered the distribution and variation of DON observed in this area.

PN produces DON mainly through cell lysis, exudation, and particle solubilization (Bronk and Steinberg, 2008). These processes are more likely to occur with the rupture of the C–C

bond but are much less likely to occur with the rupture of the C–N bond. Thus, the process of producing DON from PN would not cause a significant isotope fractionation, and the produced $\delta^{15}N$–DON should be similar to the $\delta^{15}N$ of PN from which DON is derived (Knapp et al., 2011). The $\delta^{15}N$–PN ranged from 0.7 to 7.1‰, with an average of 3.2 ± 1.8 ‰. This was slightly higher than that of $\delta^{15}N$–DON (0.1 to 5.5‰, average 2.9 ± 1.6 ‰) in P-zone 2. The mean values of the $\delta^{15}N$–PN and $\delta^{15}N$–DON in P-zone 2 showed a statistically significant difference (ANOVA, $p < 0.01$). This difference explains why the DON in P-zone 2 correlates positively with $\delta^{15}N$–DON ($R^2 = 0.29$, $p \le 0.001$, $n = 40$, **Supplementary Figure S4B**). The addition of PN-sourced DON elevated the $\delta^{15}N$–DON in the water column.

4.3 Net Consumption of DON

4.3.1 DON Consumption in NO_3^- Depleted C-Zone 1

DON is known as a potential source of N-nutrient for phytoplankton (Knapp et al., 2018). Hu et al. (2012) demonstrated the ability of *Prorocentrum donghaiense*, which frequently occurs in CEECS, to assimilate DON. Moreover, Zhang et al. (2015) suggested that DON is bioavailable during the diatom to dinoflagellate bloom succession. Thus, in C-zone 1 where NO_3^- is completely consumed, DON may play an important role in fueling phytoplankton growth. The bio-active N released from DON in C-zone 1 likely occurs with isotope fractionation when hydrolysis reactions break common C–N bonds (Knapp et al., 2011). Since DON can be continuously supplied by water mixing in the horizontal direction, a steady-state model (Eq. 6 applied to the reactant N pool) would fit the continuous DON supply and removal. The isotope effect ($^{15}\epsilon_{ass-DON}$) during DON consumption in C-zone 1 was estimated to be 3.7 ± 1.2‰ (**Figure 7A**), which is in accordance with the isotope effect (3–10‰) of the conversion of amide to amine and amine to ammonia (O'Leary and Kluetz, 1972; Macko et al., 1986; Silfer et al., 1992). The result was slightly lower than the isotope effect of 4.9 ± 0.4‰ during DON consumption in the upper layers of South China Sea (Zhang et al., 2020) and 5.5 ± 1.2‰ in the upper 50 m of Eastern Tropical South Pacific (Knapp et al., 2018). This could result from the residence time of DON that determines the extent of DON consumption. Previous studies suggested that the residence time ranged from days to months in C-zone 1 (Gu et al., 2012; Tan et al., 2018; Wang et al., 2018). In other words, DON has a shorter residence time in this area than in the upper layers of South China Sea (~3 years; Liu and Gan, 2017) or the upper ocean of Eastern Tropical South Pacific (months to years; Knapp et al., 2011). Hopkinson et al. (2002) showed that the average half-lives of very labile and labile DON are 12 and 113 days, respectively. We infer that the labile DON is not completely consumed due to the short residence time in C-zone 1. Therefore, the isotope fractionation of labile DON consumption in C-zone 1 is weaker than that of refractory DON consumption.

4.3.2 DON Consumption in NO_3^- Regenerated C-Zone 2

In C-zone 2, the enrichment ratio of ^{18}O and ^{15}N from the potential NO_3^- sources deviated from the slope of 1.0, spreading over the range from 1.0 to 2.0 (**Supplementary Figure S8A**,

Granger et al., 2004). This suggests that continuous nitrification occurred in this area (Umezawa et al., 2014; Wang et al., 2016). The negative correlation between the AOU and DON concentrations ($R^2 = 0.28$, $p = 0.001$, $n = 36$, **Supplementary Figure S5A**) and the significantly positive correlation between AOU and NO_3^- concentrations ($R^2 = 0.64$, $p < 0.001$, $n = 36$, **Supplementary Figure S5B**) suggest the aerobic microbial degradation of DON to be associated with NO_3^- regeneration and a coupling between the consumption of DON pools and the production of NO_3^- in C-zone 2. The DON remineralization and nitrification elevate the NO_3^- concentration (Liu et al., 2020).

We use the steady-state model (Eq. 6 applied to the reactant N pool) to estimate the isotope effect during DON consumption. The slope of the linear regression yielded an estimate for $^{15}\epsilon_{ntr-DON}$ of 5.6 ± 2.6‰ (**Figure 7B**). The $^{15}\epsilon_{ntr-DON}$ was consistent with the isotope effect of 5.5 ± 1.2‰ for the DON degradation estimated from data for the upper 50 m of Eastern Tropical South Pacific (Knapp et al., 2018), where the residence time was many months to years (Knapp et al., 2018). In C-zone 2, KBBCNT makes the highest contribution (>50%, **Supplementary Figure S3**). The shelf water exchange with Kuroshio Current is 1–2.3 years [summarized in Chen (1996)], which indicates that DON in C-zone 2 undergoes a longer period of degradation than in C-zone 1. As a result, DON degrades more thoroughly, and the remaining DON is more refractory. The $\delta^{15}N_{initial}$ (y-intercept) was 4.2 ± 0.3‰, which is slightly lower than the average value (4.7 ± 0.2‰) of the expected $\delta^{15}N$ values (theoretical value derived from physical mixing; Eq. 5) for DON in C-zone 2. The 0.5‰ difference may result from DON originating from "fresh" PN in C-zone 2. The isotope $\delta^{13}C$ is a useful proxy to discriminate the sources of POC. In C-zone 2, $\delta^{13}C$ averaged −21.9 ± 1.1‰, suggesting that marine phytoplankton was the predominant origin of POC (−22 to −18‰; Middelburg and Nieuwenhuize, 1998). The linear relationship between POC and PN ($R^2 = 0.91$, $p \le 0.001$, $n = 36$, **Supplementary Figure S8B**) suggests that PN was strongly associated with POC. The C/N molar ratio between POC and PN was 5.5 ± 0.3, which is lower than the Redfield ratio of 6.6 (Redfield, 1960), suggesting that the PN was "fresh" (Liu et al., 2019). The solubilization of PN is an important source of DON (Benner and Amon, 2015). The $\delta^{15}N$–PN ranged from 0.6 to 6.1‰, with an average of 3.3 ± 1.6 ‰, which was lighter than that of $\delta^{15}N$–DON (3.0 to 6.7‰, averaged 4.7 ± 0.9 ‰) in the C-zone 2. The mean values of $\delta^{15}N$–PN and $\delta^{15}N$-DON in the C-zone 2 showed a statistically significant difference (ANOVA, $p < 0.01$). As mentioned in **Section 4.2.2**, the $\delta^{15}N$ of DON produced was similar to the $\delta^{15}N$–PN. Thus, the addition of DON from PN would decrease the expected $\delta^{15}N$–DON in C-zone 2. Therefore, we suggested that the expected $\delta^{15}N$–DON had already been substantially modified by DON originating from "fresh" PN. In this section, we estimated the isotope effect during DON consumption and clarified the confounding coupling of NO_3^-, DON, and PN in the N cycling in C-zone 2.

4.3.3 Ongoing Challenges at the Remaining Sites

The remaining sites not included in these four zones are concentrated in coastal surface waters ($n = 17$, **Figure 6B**, gray

dots), where the *Error-DON* was relatively low (−3.3 ± 3.5%). Substantial challenges still exist for studying DON cycling in this zone. On the one hand, it is still uncertain whether this deviation is caused by biological processes or uncertainties for calculation. On the other hand, both the NO_3^- and PN concentrations were high in this zone, and the variation caused by DON consumption was relatively small. Understanding of the particularly complex and overlapping interactions between NO_3^-, PN, and DON remains elusive. Further studies are required to investigate this issue.

4.4 Conceptual View of DON Cycling in the CEECS

DON is a dominant dynamic component in N cycling, significantly contributing to the hypoxia and eutrophication burden in CEECS. The biochemical cycling of DON, such as mineralization and nitrification, is often accompanied by oxygen consumption and NO_3^- regeneration (Liu et al., 2020). The NO_3^- produced by DON mineralization participates in the next cycle of photosynthesis in Redfield stoichiometry. In this manner, DON mineralization plays an important role in stimulating carbon fixation. Nitrification is often accompanied by the side-production of nitrous oxide, a very powerful greenhouse gas (Yang et al., 2020). To summarize, DON cycling is closely associated with local nutrient biogeochemistry, primary productivity, and ecosystem health. A clear model of the DON cycling processes in estuaries and marginal seas is urgently needed in current marine science.

We integrated the above-mentioned results to construct the first diagram of DON cycling in the CEECS (**Figure 8**). The riverine terrestrial-derived DON input into the coastal zone undergoes substantial modifications by shelf-offshore autochthonous biological processes and degradation processes. In the CE coastal areas (P-zone 2), an area of high SPM provides the ideal location for the inter-transformation between DON and PN. The $\delta^{15}N$–PN is higher than $\delta^{15}N$–DON in this area. The DON of the PN source mixes with the local DON inventory and results in an elevation of the $\delta^{15}N$-DON in the water column. In DON P-zone 1, phytoplankton-originating DON has a low $\delta^{15}N$ and offsets the $\delta^{15}N$-DON in the water column. In the NO_3^- depleted surface seawater (C-zone 1), DON serves as a potential N source for phytoplankton assimilation or heterotrophic microbial processes. In KBBCNT (C-zone 2), continuous DON mineralization and nitrification not only replenish the NO_3^- pool but also consume oxygen. This oxygen consumption in the water column probably contributes to coastal hypoxia. In C-zone 1 or C-zone 2, incomplete DON consumption (N released from DON) elevates the $\delta^{15}N$ of residual DON relative to the original $\delta^{15}N$. The isotope effect was estimated to be 3.7 ± 1.2‰ and 5.6 ± 2.6‰. Based on these results, we suggest that the longer the residence time is, the more completely the DON degrades and the stronger is the isotope effect. This DON cycling diagram (**Figure 8**) not only fits the CEECS but also is appropriate to be used to describe DON cycling in many other estuarine and marginal marine systems, even though the relative intensities of DON cycling processes may vary.
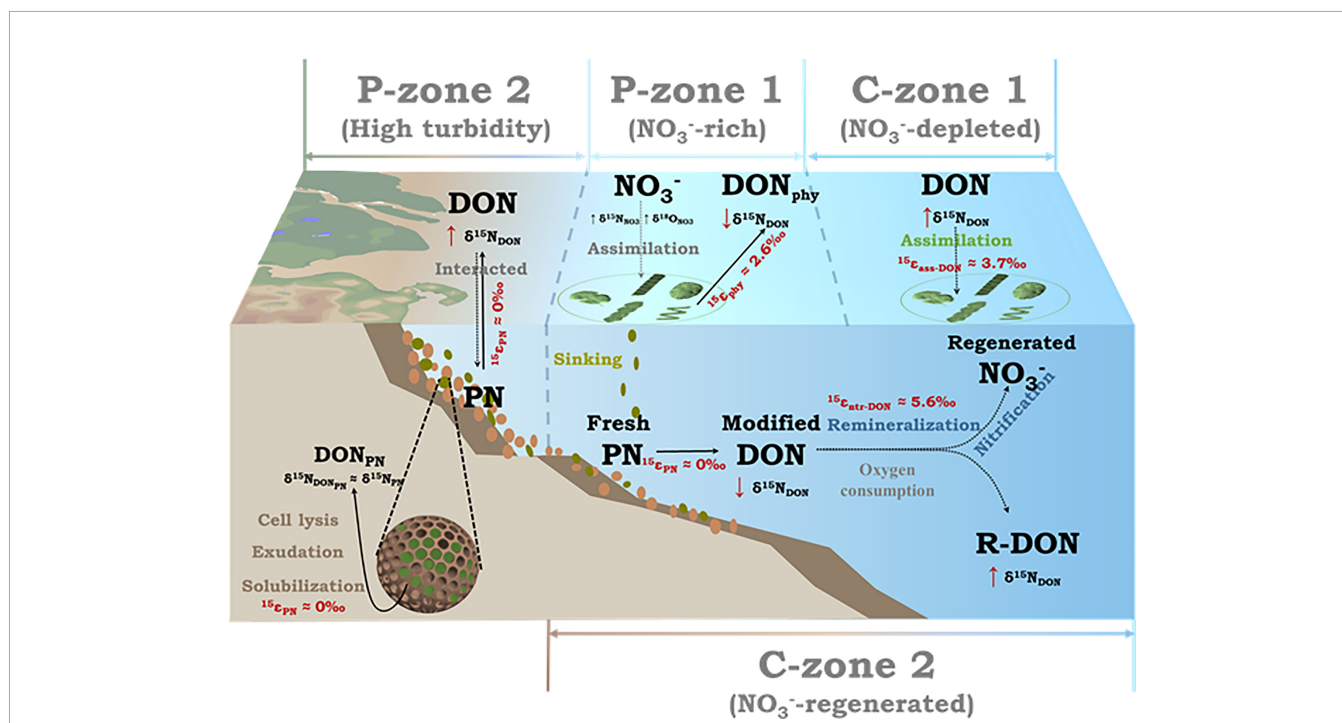
FIGURE 8 | Diagram of dissolved organic nitrogen production and consumption in the Changjiang Estuary and the adjacent East China Sea shelf areas with a description of the reaction pathways. The dotted arrow represents the consumption process, and the solid arrow represents the production process.

5 CONCLUSIONS

This study proved that DON is an active component in N cycling in estuaries and global marginal seas. Intensive physical processes are among the major drivers controlling the distribution of DON, but the active biotic processes as well play an important role, as revealed and evidenced by the results of the OMP analysis combined with information on the $\delta^{15}N$ of DON and other associated N species. There exists dynamic zoning in DON production and consumption in the direction from the estuary to the offshore marginal sea. The combination of OMP analysis and multiple N isotopic proxies has proven to be a useful means of studying DON cycling and may help to improve understanding of the complicated DON dynamics in perturbed estuaries and adjacent marginal seas on a global scale.

DATA AVAILABILITY STATEMENT

The datasets presented in this study can be found in an online repository. The name of the repository and accession number can be found below: https://doi.org/10.6084/m9.figshare.17170967.v1.

AUTHOR CONTRIBUTIONS

XZ: conceptualization, methodology, Investigation, data curation, visualization, and writing—original draft. MY, WX, ZY, FX, and SD: investigation and data curation. YX: conceptualization, methodology, writing—review and editing, supervision, and funding acquisition. XS: conceptualization and supervision. All authors contributed to the article and approved the submitted version.

FUNDING

ACKNOWLEDGMENTS

SUPPLEMENTARY MATERIAL

The Supplementary Material for this article can be found online at: https://www.frontiersin.org/articles/10.3389/fmars.2022.855479/full#supplementary-material

REFERENCES

Benner, R., and Amon, R. M. W. (2015). The Size-Reactivity Continuum of Major Bioelements in the Ocean. *Annu. Rev. Mar. Sci.* 7 (1), 185–205. doi: 10.1146/annurev-marine-010213-135126

Berman, T., and Bronk, D. A. (2003). Dissolved Organic Nitrogen: A Dynamic Participant in Aquatic Ecosystems. *Aquat. Microbial Ecol.* 31 (3), 279–305. doi: 10.3354/ame031279

Braman, R. S., and Hendrix, S. A. (1989). Nanogram Nitrite and Nitrate Determination in Environmental and Biological Materials by Vanadium(III) Reduction With Chemiluminescence Detection. *Anal. Chem.* 61 (24), 2715–2718. doi: 10.1021/ac00199a007

Bronk, D. A. (2002). "Dynamics of DON," in *Biogeochemistry of Marine Dissolved Organic Matter* (New York: Academic Press) pp. 153–247. doi: 10.1016/b978-012323841-2/50007-5

Bronk, D. A., See, J. H., Bradley, P., and Killberg, L. (2007). DON as a Source of Bioavailable Nitrogen for Phytoplankton. *Biogeosciences* 4 (3), 283–296. doi: 10.5194/bg-4-283-2007

Bronk, D. A., and Steinberg, D. K. (2008). "Nitrogen Regeneration," in *Nitrogen in the Marine Environment* (New York: Academic Press) pp. 385–467. doi: 10.1016/B978-0-12-372522-6.00008-6

Budillon, G., Pacciaroni, M., Cozzi, S., Rivaro, P., Catalano, G., Ianni, C., et al. (2003). An Optimum Multiparameter Mixing Analysis of the Shelf Waters in the Ross Sea. *Antar. Sci.* 15 (1), 105–118. doi: 10.1017/S095410200300110X

Chen, T. (1996). The Kuroshio Intermediate Water Is the Major Source of Nutrients on the East China Sea Continental Shelf. *Oceanolog Acta* 19 (5), 523–527.

Chen, C. T. A. (2009). Chemical and Physical Fronts in the Bohai, Yellow and East China Seas. *J. Mar. Syst.* 78 (3), 394–410. doi: 10.1016/j.jmarsys.2008.11.016

Chen, C. T. A., Kandasamy, S., Chang, Y. P., Bai, Y., He, X., Lu, J. T., et al. (2017). Geochemical Evidence of the Indirect Pathway of Terrestrial Particulate Material Transport to the Okinawa Trough. *Quater. Int.* 441 (Part A), 51–61. doi: 10.1016/j.quaint.2016.08.006

Dai, Z., Du, J., Zhang, X., Su, N., and Li, J. (2011). Variation of Riverine Material Loads and Environmental Consequences on the Changjiang (Yangtze) Estuary in Recent Decades, (1955-2008). *Environ. Sci. Technol.* 45 (1), 223–227. doi: 10.1021/es103026a

de Carvalho Ferreira, M. L., and Kerr, R. (2017). Source Water Distribution and Quantification of North Atlantic Deep Water and Antarctic Bottom Water in the Atlantic Ocean. *Prog. Oceanog.* 153, 66–83. doi: 10.1016/j.pocean.2017.04.003

Gao, L., Gao, Y., Song, S., and Zhang, F. (2020). Non-Conservative Behavior of Dissolved Organic Carbon in the Changjiang (Yangtze River) Estuary and the Adjacent East China Sea. *Continent. Shelf. Res.* 197, 104084. doi: 10.1016/j.csr.2020.104084

Gasparin, F., Maes, C., Sudre, J., Garcon, V., and Ganachaud, A. (2014). Water Mass Analysis of the Coral Sea Through an Optimum Multiparameter Method. *J. Geophys. Res.: Ocean.* 119 (10), 7229–7244. doi: 10.1002/2014JC010246

Gebhardt, A. C., Schoster, F., Gaye-Haake, B., Beeskow, B., Rachold, V., Unger, D., et al. (2005). The Turbidity Maximum Zone of the Yenisei River (Siberia) and its Impact on Organic and Inorganic Proxies. *Estuarine Coast. Shelf. Sci.* 65 (1–2), 61–73. doi: 10.1016/j.ecss.2005.05.007

Granger, J., and Sigman, D. M. (2009). Removal of Nitrite With Sulfamic Acid for Nitrate N and O Isotope Analysis With the Denitrifier Method. *Rapid Commun. Mass. Spectromet.* 23 (23), 3753–3762. doi: 10.1002/rcm.4307

Granger, J., Sigman, D. M., Needoba, J. A., and Harrison, P. J. (2004). Coupled Nitrogen and Oxygen Isotope Fractionation of Nitrate During Assimilation by

Cultures of Marine Phytoplankton. *Limnol. Oceanog.* 49 (5), 1763–1773. doi: 10.4319/lo.2004.49.5.1763

Gu, H., Moore, W. S., Zhang, L., Du, J., and Zhang, J. (2012). Using Radium Isotopes to Estimate the Residence Time and the Contribution of Submarine Groundwater Discharge (SGD) in the Changjiang Effluent Plume, East China Sea. *Continent. Shelf. Res.* 35, 95–107. doi: 10.1016/J.CSR.2012.01.002

Hansen, H. P., and Koroleff, F. (2007). "Determination of Nutrients," in *Methods of Seawater Analysis: Third, Completely Revised and Extended Edition.* Eds. K. Grasshoff, K. Kremling and M. Ehrhardt (Weinheim: John Wiley & Sons), (pp. 159–228). doi: 10.1002/9783527613984.ch10

He, Q., Qiu, Y., Liu, H., Sun, X., Kang, L., Cao, L., et al. (2017). New Insights Into the Impacts of Suspended Particulate Matter on Phytoplankton Density in a Tributary of the Three Gorges Reservoir, China. *Sci. Rep.* 7 (1), 13518. doi: 10.1038/s41598-017-13235-0

Holmes, R. M., Aminot, A., Kérouel, R., Hooker, B. A., and Peterson, B. J. (1999). A Simple and Precise Method for Measuring Ammonium in Marine and Freshwater Ecosystems. *Can. J. Fish. Aquat. Sci.* 56 (10), 1801–1808. doi: 10.1139/f99-128

Hopkinson, C. S., Vallino, J. J., and Nolin, A. (2002). Decomposition of Dissolved Organic Matter From the Continental Margin. *Deep-Sea Research Part Ii. Top. Stud. Oceanog.* 49 (20), 4461–4478. doi: 10.1016/S0967-0645(02)00125-X

Hou, W., Ba, M., Bai, J., and Yu, J. (2021). Numerical Study on the Expansion and Variation of Changjiang Diluted Water in Summer and Autumn. *J. Mar. Sci. Eng.* 9 (3), 317. doi: 10.3390/jmse9030317

Hu, Z., Mulholland, M. R., Duan, S., and Xu, N. (2012). Effects of Nitrogen Supply and its Composition on the Growth of Prorocentrum Donghaiense. *Harm. Algae.* 13, 72–82. doi: 10.1016/j.hal.2011.10.004

Jani, J., and Toor, G. S. (2018). Composition, Sources, and Bioavailability of Nitrogen in a Longitudinal Gradient From Freshwater to Estuarine Waters. *Water Res.* 137, 344–354. doi: 10.1016/j.watres.2018.02.042

Kim, J., Kim, T. H., Park, S. R., Lee, H. J., and Kim, J. K. (2020). Factors Controlling the Distributions of Dissolved Organic Matter in the East China Sea During Summer. *Sci. Rep.* 10 (1), 11854. doi: 10.1038/s41598-020-68863-w

Knapp, A. N., Casciotti, K. L., and Prokopenko, M. G. (2018). Dissolved Organic Nitrogen Production and Consumption in Eastern Tropical South Pacific Surface Waters. *Global Biogeochem. Cycle.* 32 (5), 769–783. doi: 10.1029/2017GB005875

Knapp, A. N., Sigman, D. M., and Lipschultz, F. (2005). N Isotopic Composition of Dissolved Organic Nitrogen and Nitrate at the Bermuda Atlantic Time-Series Study Site. *Global Biogeochem. Cycle.* 19 (1), 1–15. doi: 10.1029/2004GB002320

Knapp, A. N., Sigman, D. M., Lipschultz, F., Kustka, A. B., and Capone, D. G. (2011). Interbasin Isotopic Correspondence Between Upper-Ocean Bulk DON and Subsurface Nitrate and its Implications for Marine Nitrogen Cycling. *Global Biogeochem. Cycle.* 25 (4), GB4004. doi: 10.1029/2010GB003878

Kwon, H. K., Kim, G., Hwang, J., Lim, W. A., Park, J. W., and Kim, T. H. (2018). Significant and Conservative Long-Range Transport of Dissolved Organic Nutrients in the Changjiang Diluted Water. *Sci. Rep.* 8 (1), 12768. doi: 10.1038/s41598-018-31105-1

Letscher, R. T., Hansell, D. A., Carlson, C. A., Lumpkin, R., and Knapp, A. N. (2013). Dissolved Organic Nitrogen in the Global Surface Ocean: Distribution and Fate. *Global Biogeochem. Cycle.* 27 (1), 141–153. doi: 10.1029/2012GB004449

Lim, J. H., Wong, Y. Y., Lee, C. W., Bong, C. W., and Kudo, I. (2019). Long-Term Comparison of Dissolved Nitrogen Species in Tropical Estuarine and Coastal Water Systems. *Estuarine Coast. Shelf. Sci.* 222, 103–111. doi: 10.1016/j.ecss.2019.04.008

Liu, X., Beusen, A. H. W., Van Beek, L. P. H., Mogollón, J. M., Ran, X., and Bouwman, A. F. (2018). Exploring Spatiotemporal Changes of the Yangtze River (Changjiang) Nitrogen and Phosphorus Sources, Retention and Export to the East China Sea and Yellow Sea. *Water Res.* 142 (1), 246–255. doi: 10.1016/j.watres.2018.06.006

Liu, Z., and Gan, J. (2017). Three-Dimensional Pathways of Water Masses in the South China Sea: A Modeling Study. *J. Geophys. Res.: Ocean.* 122 (7), 6039–6054. doi: 10.1002/2016JC012511

Liu, Z., Gan, J., Wu, H., Hu, J., Cai, Z., and Deng, Y. (2021). Advances on Coastal and Estuarine Circulations Around the Changjiang Estuary in the Recent Decades, (2000–2020). *Front. Mar. Sci.* 8. doi: 10.3389/fmars.2021.615929

Liu, Q., Kandasamy, S., Wang, H., Wang, L., Lin, B., Gao, A., et al. (2019). Impact of Hydrological Conditions on the Biogeochemical Dynamics of Suspended Particulate Organic Matter in the Upper Mixed Layer of the Southern East China Sea. *J. Geophys. Res. Ocean.* 124 (8), 6120–6140. doi: 10.1029/2019JC015193

Liu, S. M., Ning, X., Dong, S., Song, G., Wang, L., Altabet, M. A., et al. (2020). Source Versus Recycling Influences on the Isotopic Composition of Nitrate and Nitrite in the East China Sea. *J. Geophys. Res.: Ocean.* 125 (8), e2020JC016061. doi: 10.1029/2020JC016061

Liu, S. M., Qi, X. H., Li, X., Ye, H. R., Wu, Y., Ren, J. L., et al. (2016). Nutrient Dynamics From the Changjiang (Yangtze River) Estuary to the East China Sea. *J. Mar. Syst.* 154, 15–27. doi: 10.1016/j.jmarsys.2015.05.010

Liu, X., Yu, Z., Song, X., and Cao, X. (2009). The Nitrogen Isotopic Composition of Dissolved Nitrate in the Yangtze River (Changjiang) Estuary, China. *Estuarine Coast. Shelf. Sci.* 85 (4), 641–650. doi: 10.1016/j.ecss.2009.09.017

Macko, S. A., Estep, M. L. F., Engel, M. H., and Hare, P. E. (1986). Kinetic Fractionation of Stable Nitrogen Isotopes During Amino Acid Transamination. *Geochim. Cosmochim. Acta* 50 (10), 2143–2146. doi: 10.1016/0016-7037(86)90068-2

Mao, H. (1964). A Preliminary Investigation on the Application of Using T-S Diagram for a Quantitative Analysis of the Water Masses in the Shallow Water Area. *Oceanolog. Limnol. Sin.* 6 (1–22), 1–22.

Middelburg, J. J., and Nieuwenhuize, J. (1998). Carbon and Nitrogen Stable Isotopes in Suspended Matter and Sediments From the Schelde Estuary. *Mar. Chem.* 60 (3–4), 217–225. doi: 10.1016/S0304-4203(97)00104-7

Moon, J. Y., Lee, K., Lim, W. A., Lee, E., Dai, M., Choi, Y. H., et al. (2021). Anthropogenic Nitrogen is Changing the East China and Yellow Seas From Being N Deficient to Being P Deficient. *Limnol. Oceanog.* 66 (3), 914–924. doi: 10.1002/lno.11651

O'Leary, M. H., and Kluetz, M. D. (1972). Nitrogen Isotope Effects on the Chymotrypsin-Catalyzed Hydrolysis of jV-Acetyl-L-Tryptophanamide. *J. Am. Chem. Soc.* 94 (10), 3585–3589. doi: 10.1021/ja00765a055

Poole, R., and Tomczak, M. (1999). Optimum Multiparameter Analysis of the Water Mass Structure in the Atlantic Ocean Thermocline. *Deep-Sea Research Part I. Oceanog. Res. Pap.* 46 (11), 1895–1921. doi: 10.1016/S0967-0637(99)00025-4

Redfield, A. C. (1960). The Biological Control of Chemical Factors in the Environment. *Sci. Prog.* 11 (3), 150–170.

Sigman, D. M., Casciotti, K. L., Andreani, M., Barford, C., Galanter, M., and Böhlke, J. K. (2001). A Bacterial Method for the Nitrogen Isotopic Analysis of Nitrate in Seawater and Freshwater. *Anal. Chem.* 73 (17), 4145–4153. doi: 10.1021/ac010088e

Sigman, D. M., and Fripiat, F. (2019). "Nitrogen Isotopes in the Ocean," in *Encyclopedia of Ocean Sciences* (New York: Academic Press) pp. 263–278. doi: 10.1016/B978-0-12-409548-9.11605-7

Sigman, D. M., Karsh, K. L., and Casciotti, K. L. (2009). "Nitrogen Isotopes in the Ocean," in *Encyclopedia of Ocean Sciences* (New York: Academic Press) pp. 40–54. doi: 10.1016/B978-012374473-9.00632-9

Silfer, J. A., Engel, M. H., and Macko, S. A. (1992). Kinetic Fractionation of Stable Carbon and Nitrogen Isotopes During Peptide Bond Hydrolysis: Experimental Evidence and Geochemical Implications. *Chem. Geol.* 101 (3–4), 211–221. doi: 10.1016/0009-2541(92)90003-N

Sipler, R. E., and Bronk, D. A. (2015). "Dynamics of Dissolved Organic Nitrogen," in *Biogeochemistry of Marine Dissolved Organic Matter: Second Edition*, (New York: Academic Press) pp. 127–232). doi: 10.1016/B978-0-12-405940-5.00004-2

Su, Y., and Weng, X. (1994). "Water Masses in China Seas," in *Oceanology of China Seas* (Dordrecht: Springer) pp. 3–16. doi: 10.1007/978-94-011-0862-1_2

Tan, E., Wang, G., Moore, W. S., Li, Q., and Dai, M. (2018). Shelf-Scale Submarine Groundwater Discharge in the Northern South China Sea and East China Sea and its Geochemical Impacts. *J. Geophys. Res.: Ocean.* 123 (4), 2997–3013. doi: 10.1029/2017JC013405

Tomczak, M., and Large, D. G. B. (1989). Optimum Multiparameter Analysis of Mixing in the Thermocline of the Eastern Indian Ocean. *J. Geophys. Res.* 94 (C11), 16141. doi: 10.1029/jc094ic11p16141

Umezawa, Y., Yamaguchi, A., Ishizaka, J., Hasegawa, T., Yoshimizu, C., Tayasu, I., et al. (2014). Seasonal Shifts in the Contributions of the Changjiang River and

the Kuroshio Current to Nitrate Dynamics in the Continental Shelf of the Northern East China Sea Based on a Nitrate Dual Isotopic Composition Approach. *Biogeosciences* 11 (4), 1297–1317. doi: 10.5194/bg-11-1297-2014

Wang, X., Baskaran, M., Su, K., and Du, J. (2018). The Important Role of Submarine Groundwater Discharge (SGD) to Derive Nutrient Fluxes Into River Dominated Ocean Margins – The East China Sea. *Mar. Chem.* 204, 121–132. doi: 10.1016/J.MARCHEM.2018.05.010

Wang, H., Dai, M., Liu, J., Kao, S. J., Zhang, C., Cai, W. J., et al. (2016). Eutrophication-Driven Hypoxia in the East China Sea Off the Changjiang Estuary. *Environ. Sci. Technol.* 50 (5), 2255–2263. doi: 10.1021/acs.est.5b06211

Wang, W., Yu, Z., Song, X., Wu, Z., Yuan, Y., Zhou, P., et al. (2016). The Effect of Kuroshio Current on Nitrate Dynamics in the Southern East China Sea Revealed by Nitrate Isotopic Composition. *J. Geophys. Res.: Ocean.* 121 (9), 7073–7087. doi: 10.1002/2016JC011882

Weigand, M. A., Foriel, J., Barnett, B., Oleynik, S., and Sigman, D. M. (2016). Updates to Instrumentation and Protocols for Isotopic Analysis of Nitrate by the Denitrifier Method. *Rapid Commun. Mass. Spectromet.* 30 (12), 1365–1383. doi: 10.1002/rcm.7570

Yang, S., Chang, B. X., Warner, M. J., Weber, T. S., Bourbonnais, A. M., Santoro, A. E., et al. (2020). Global Reconstruction Reduces the Uncertainty of Oceanic Nitrous Oxide Emissions and Reveals a Vigorous Seasonal Cycle. *Proc. Natl. Acad. Sci. U. S. A.* 117 (22), 11954. doi: 10.1073/pnas.1921914117

Yang, D., Yin, B., Liu, Z., and Feng, X. (2011). Numerical Study of the Ocean Circulation on the East China Sea Shelf and a Kuroshio Bottom Branch Northeast of Taiwan in Summer. *J. Geophys. Res.: Ocean.* 116 (5), C05015. doi: 10.1029/2010JC006777

Zhang, J., Du, Y. N., Zhang, G. S., Chang, Y., Zhou, Y. C., Zhang, Z. F., et al. (2021). Increases in the Seaward River Flux of Nutrients Driven by Human Migration and Land-Use Changes in the Tide-Influenced Delta. *Sci. Total Environ.* 761 (20), 144501. doi: 10.1016/j.scitotenv.2020.144501

Zhang, S., Ji, H., Yan, W., and Duan, S. (2003). Composition and Flux of Nutrients Transport to the Changjiang Estuary. *J. Geogr. Sci.* 13 (1), 3–12. doi: 10.1007/bf02873141

Zhang, G., Liang, S., Shi, X., and Han, X. (2015). Dissolved Organic Nitrogen Bioavailability Indicated by Amino Acids During a Diatom to Dinoflagellate Bloom Succession in the Changjiang River Estuary and its Adjacent Shelf. *Mar. Chem.* 176 (20), 83–95. doi: 10.1016/j.marchem.2015.08.001

Zhang, R., Wang, X. T., Ren, H., Huang, J., Chen, M., and Sigman, D. M. (2020). Dissolved Organic Nitrogen Cycling in the South China Sea From an Isotopic Perspective. *Global Biogeochem. Cycle.* 34 (12), e2020GB006551. doi: 10.1029/2020GB006551

Zhong, X., Yan, M., Ning, X., Yan, Z., and Xin, Y. (2020). Nitrate Processing Traced by Nitrate Dual Isotopic Composition in the Early Spring in the Changjiang (Yangtze River) Estuary and Adjacent Shelf Areas. *Mar. Pollution Bull.* 161 (Part A), 111699. doi: 10.1016/j.marpolbul.2020.111699

Zhou, P., Song, X., Yuan, Y., Cao, X., Wang, W., Chi, L., et al. (2018). Water Mass Analysis of the East China Sea and Interannual Variation of Kuroshio Subsurface Water Intrusion Through an Optimum Multiparameter Method. *J. Geophys. Res.: Ocean.* 123 (5), 3723–3738. doi: 10.1029/2018JC013882

Zhu, C., Wang, Z. H., Xue, B., Yu, P. S., Pan, J. M., Wagner, T., et al. (2011). Characterizing the Depositional Settings for Sedimentary Organic Matter Distributions in the Lower Yangtze River-East China Sea Shelf System. *Estuarine Coast. Shelf. Sci.* 93 (3), 182–191. doi: 10.1016/j.ecss.2010.08.001